Review Article

Doris Ehrt[a,*]

Deep-UV materials

https://doi.org/10.1515/aot-2018-0023
Received April 24, 2018; accepted May 24, 2018; previously published online June 18, 2018

Abstract: Materials with high deep-ultraviolet (DUV; $\lambda < 300$ nm) transmission are important for many industrial applications. Fluoride single crystals and various glasses, pure SiO_2, fluoride, phosphate, multicomponent silicates, and organic materials (PMMA), were investigated. The role of intrinsic absorption (UV edge) due to electron transitions between the main components, and extrinsic absorption due to trace impurities, effect of polyvalent ions, redox behavior, and radiation-induced transmission loss were considered. The optical basicity and optical properties were used to order the materials.

Keywords: bandgaps; crystals; deep-UV transmission; glasses; impurities; optical basicity; radiation defects.

OCIS codes: 160.0160; 160.2750; 160.3220; 160.4670; 170.6280

1 Introduction

The demand for deep-ultraviolet (DUV $\lambda < 300$ nm) transmitting materials increased at the end of the 1980s especially for lens systems in microlithography equipment, for windows, lens blanks and substrate materials for excimer laser system optics, for space applications, for fiber optics, and for solid state laser applications. Various UV-light sources are also used for disinfection, sterilization, surface cleaning, vapor deposition, and detection of traces. Mercury, xenon, and excimer discharge lamps, e.g. Xe (172 nm), KrCl (222 nm), and XeBr (282 nm), are of interest. Typical operating wavelengths of excimer lasers are 351 nm (XeF), 308 nm (XeCl), 248 nm (KrF), 193 nm (ArF), and 157 nm (F_2). Furthermore, the wavelengths generated by frequency conversion of the fundamental laser wavelength 1064 nm of Nd:YAG are important, e.g. 266 nm = 1064 nm/4 fourth-harmonic generation (FOHG), 177.3 nm = 1064 nm/6 sixth-harmonic generation (6thHG). Different materials with high transmission and low damage for these wavelengths are required. Fluoride single crystals, like CaF_2, BaF_2 and MgF_2, and vitreous SiO_2 are well-known traditional materials for the use in the DUV region [1–3]. The disadvantages for single crystals are the limitation in crystal sizes, the length of time (up to many weeks) for crystal growth, crystal imperfections, and preferential cleavage, which leads to more difficult fabrication of optical surfaces. Vitreous silica can be produced as 'fused silica' by melting quartz crystals, which have trace impurities, or with extremely high purity as 'synthetic silica' by the CVD (chemical vapor deposition) process of $SiCl_4$ hydrolysis in different ways. Depending on start materials and fabrication technology, various SiO_2 glass types with different properties can be commercially produced. Brückner classified SiO_2 glass as types I, II, III, IIIa, IIIb, IV, V, VI, and VII, depending on the manufacturing methods [4]. Temperatures greater than 2000°C are necessary for the electric melting of quartz crystals in a crucible under vacuum or by H_2/O_2 flame fusion. The melts have very high viscosity. The homogenization process by stirring the melt, used in other glass melts with lower melting temperature and lower viscosity, is not possible. It is difficult to introduce dopants, e.g. rare earth ions, into the SiO_2 glass network in a homogeneous distribution without clustering. Moreover, for optical lens systems, a variety of glasses with different optical properties is required. Fluoride phosphate (FP) glasses are attractive candidates as DUV transmitting materials. Their intrinsic UV edge is comparable with those of silica [2, 5–7]. However, they consist of many components, e.g. AlF_3, CaF_2, SrF_2, BaF_2, MgF_2, P_2O_5, etc., and their raw materials are not available in super high purity. The actual UV transmission of glasses is frequently limited by trace impurities, mainly polyvalent ions in different redox states, introduced by raw materials, and possible contamination from the melting technique and processing method. We have studied this effect very extensively [2, 5–16].

The intrinsic UV absorption edge of multicomponent silicate glasses is shifted to longer wavelengths

[a]Private address: Rudolf-Breitscheid-Str. 51, D-07747 Jena, Germany
***Corresponding author: Doris Ehrt,** Otto-Schott-Institute, Friedrich-Schiller-Universität Jena, Fraunhoferstr. 6, D-07743 Jena, Germany, e-mail: doris.ehrt@uni-jena.de

depending on their optical basicity (Duffy: electron donor power [17–19]), which can be mainly correlated with the content of nonbridging oxygen of the glass structure.

When materials are subjected to ionizing radiation, the principal effects result from electronic processes, which are responsible for the stability against radiation-induced processes. This effect is important for different applications of the materials [7, 20–40]. The structure of various glasses was studied by different methods [7, 26, 41–52].

The aim of the paper is to give an overview of different DUV transmitting materials and to summarize specific measurements of different glasses over a long period. Different DUV materials are compared with respect to their properties and suitability for a particular application.

2 Crystals

Table 1 summarizes the approximated values of important properties of alkali and alkaline earth fluoride crystals in comparison to α-quartz given in Ref. [1]. All fluoride crystals have a very large transmission range from the vacuum ultraviolet (VUV) to the infrared (IR) spectral region. Their intrinsic VUV edge is due to electron transitions between fluorine and the alkali or alkaline earth ions. These are strong ionic bonds with very high bandgaps, decreasing with increasing ionic radius of the cations: Li^+ ~ 0.76 Å, Na^+ ~ 1.02 Å, K^+ ~ 1.38 Å, Mg^{2+} ~ 0.72 Å, Ca^{2+} ~ 1.12 Å, Sr^{2+} ~ 1.26 Å, and Ba^{2+} ~ 1.42 Å. The alkali fluorides LiF, NaF, and KF crystallize in an isotropic cubic crystal system, with low intrinsic birefringence (Δn), in a NaCl crystal lattice with coordination number six. In MgF_2, Mg^{2+} is also sixfold coordinated with F^- ions. However, it has a rutile structure in an anisotropic tetragonal crystal system, which leads to a high optical double refraction Δn (birefringence). CaF_2, SrF_2, and BaF_2 are cubic crystals with a fluorspar (fluorite) lattice and coordination number eight. The values for refractive index and density of fluoride crystals increase with increasing atomic weight of the cations. The chemical resistance of the fluoride crystals, e.g. solubility in water, is very different. MgF_2 and CaF_2 have very high resistance to water (moisture). Contrastingly, KF has a very low chemical resistance inhibiting a practical application. NaF is also hygroscopic. All fluoride single crystals possess a preferential cleavage in the lattice. Miller indices are used to denote the easiest cleavage planes in Table 1 [1].

The SiO_2 single crystal α-quartz is the stable phase with a trigonal system and consists of SiO_4 tetrahedrons connected by common oxygen in a trigonal crystal system with two refractive indices, extraordinary n_e 1.56 and ordinary n_0 1.55, and birefringence Δn 0.0095 within the crystal. The strong Si-O bonds are more covalent, and their vibrations limit the IR edge. The transmission ranges from ~0.16 μm in the VUV to 4.0 μm in the IR. The resistance to water is very high. No visible surface erosion of the crystal after long contact with water was observed. However, HF, alkaline solutions, or metal vapors attack SiO_2. The α-quartz crystals are usually fabricated by a hydrothermal process and are used as piezoelectric materials in small pieces.

LiF and MgF_2 with very low refractive index are mainly used as antireflection coating materials produced by vapor deposition. SrF_2 and BaF_2 are also commercially fabricated as bulk material for special applications. Often, they have lower DUV transmission due to trace impurities

Table 1: Properties of crystals with high DUV transmission [1].

Crystal	Transmission VUV-IR (μm)	Bandgap (eV)	Refractive index n	Density (g/cm³)	Crystal system	Cleavage plane	Solubility (°C) (g/100 g H_2O)
LiF	0.12–6.6	13.6	1.3912	2.635	Cubic	(100)-p	0.27 (18)
NaF	0.13–12	10.5	1.326	2.588	Cubic	(100)-p	4.2 (18)
KF	0.146–16	10.9	1.362	2.48	Cubic	(100)-p	92.3 (18)
MgF_2	0.13–7.7	10.8	n_e 1.3886 n_o 1.3768 Δn 0.0118	3.18	Tetragonal	(010), (110)	$<2\times10^{-4}$
CaF_2	0.12–10	10.0	1.433	3.180	Cubic	(111)-p	1.6×10^{-3} (18)
SrF_2	0.13–12	9.4	1.4371	4.24	Cubic	(111)-p	0.012 (20)
BaF_2	0.14–13	9.1	1.4733	4.83	Cubic	(111)-p	0.12
SiO_2 (α-quartz)	0.16–4.0	8.4	n_e 1.56 n_o 1.55 Δn 0.0095	2.65	Trigonal	None	Insoluble

and dislocations in the crystal lattice. BaF_2 is useful as scintillator material and as transmission window material for IR spectroscopy. Optically isotropic (cubic) crystals are used for windows and lenses. Optically anisotropic materials with wide transparency range and moderate birefringence are necessary for nonlinear optical applications, e.g. frequency conversion of the fundamental laser wavelength 1064 nm (Nd:YAG) generating 266 nm (FOHG), or 177.3 nm (6thHG). 'Easy' growth of high-quality single crystals with a second harmonic generation (SHG) coefficient larger than the value for KH_2PO_4 (KDP), and a minimum size of 5 mm^3 is necessary. It could be fluorooxoborates, e.g. $Li_2B_6O_9F$ for the shortest phase-matching wavelength at 192 nm. The calculated optical properties are very attractive for DUV NLO applications [3]. However, crystal growth is very complicated and, generally, a large problem.

The CaF_2 single crystal is the most important optical material for the DUV region grown by the optimized Czochralski method in very large dimensions and very high optical quality [53] (www.schott.com/lithotec, www.hellma-materials.com). It is used for optics in micro-lithography equipment at 248 nm and 193 nm. CaF_2 blanks, up to 440 mm in diameter and 100 mm in thickness with highest transmission down to 157 nm, are fabricated (www.schott.com/lithotec, www.hellma-materials.com). The resistance to DUV radiation is very high. The excimer laser-induced damage was intensively studied by Natura et al. [30–32].

3 Glasses

3.1 SiO_2 glasses

Vitreous SiO_2 is well known and has been used for a very long time. Generally, it can be fabricated with two different methods with strong possible variations in detail. The types described by Brückner [4] with additions [34] are briefly summarized:

1. Melting of crystalline quartz as raw material (designations: 'fused silica', 'quartz glass', 'natural quartz glass'); electric melting of natural quartz crystals in Mo or W crucibles under vacuum as type I, with lower DUV transmission due to higher impurities introduced by quartz crystals as raw material and contamination by the crucibles. Type II is produced by H_2/O_2 flame fusion of crystalline quartz. Type Va is produced by electric melting of pegmatite quartz grains in Mo or W crucibles and H_2-containing atmosphere; Vb is the same as Va but without gassing in vacuum or in air; Vc is the same as Va but melted from synthetic quartz grains. Type VI is produced by sintering colloidal SiO_2 glass powder preforms after purification by chloride reaction. Fusion of quartz crystals by a plasma arc torch is also possible (type VIII).
2. Hydrolysis of $SiCl_4$ (or other silanes) in a H_2/O_2 flame, deposition, and consolidation in the same step as type III ('synthetic silica glass'); as a variant, type IIIa: hydrolysis of $SiCl_4$ (or other silanes) in H_2/O_2 flame, deposition of soot particles to form a porous intermediate body, consolidation to full density in a separate step without dehydration; type IIIb is with dehydration of the intermediate soot body by Cl or F treatment leading to low OH-content but with introduction of Cl′ and F′. Type IV is produced by oxidation of $SiCl_4$ in a water vapor-free plasma flame.

This shows that many various types of SiO_2 glasses can be produced depending on raw materials and technologies, a sol-gel route of Si-alkoxides can also be made (as type VII), with very different properties. It can be demonstrated with specific measurements of various commercially available optical SiO_2 glass types from HERAEUS (www.optics.heraeus-quarzglas.com). Table 2 gives an overview of the glass types investigated and our measured data. Figures 1–3 show typical absorption, photoluminescence, and transmission spectra of different SiO_2 quartz glass samples fabricated with different technologies. The high absorption in the UV region, typical for these types, is caused by trace impurities, mainly alkali and alkali earth ions, in the ppbw range (Table 2) introduced by the natural quartzes as raw materials with extrinsic effects, and by the oxygen-deficient centers ODC(II) (≡Si—Si≡) (Figure 1A) absorbing at 243 nm [34, 54] due to melting conditions at very high temperatures, $T > 2000°C$, under O_2/H_2 gases, with intrinsic effects of the SiO_2 glass structure.

Photoluminescence excitation (with 150-W Xe lamp) in the ODC band provides two emission bands at 290 nm and 390 nm (Figure 1B). The OH-content is another important property, especially for the IR absorption (Figure 1C). The OH-content can be decreased by additional thermal treatment around 1200°C in vacuum, e.g. sample HSQ 100 with [OH] ~ 133 ppm, and HSQ 100 v.g. with [OH] ~ 38 ppm (Table 2). This leads to an increase in ODC(II) absorption (Figure 1A) and ODC(II) photoluminescence (Figure 1B) with visible blue color (Figure 2D).

Figure 2A and B demonstrates that the distribution of the ODC(II) in a large piece of HSQ 100 v.g. was not homogeneous. The measurements of two different smaller samples 1.1. and 1.2. (thickness 12 mm) of a large piece provided different signals for the ODC(II) with a good

Table 2: Measured properties of various SiO_2 glass samples.

Samples[a] Designation	Preparation	Density (g/cm^3) (±0.001)	Impurities (ppbw) Li Na K Mg	OH (ppmw)	Refractive index n_e ($\pm 2\times10^{-5}$)	Abbe value ν_e (±0.1)	UV-Ab. at 243 nm (cm^{-1})	Photoluminescence Excitation (nm/I^+) Emission (nm)/I^+
1 HSQ 100 v.g.	Nat. SiO_2 ODC 243 nm	nm	500 310 280 <15	38	1.1: 1.46028 1.2: 1.46023	67.8	1.1: 0.34 1.2: 0.18	246/287 290/70 390/243 /140 /35 /125
2 HSQ 100	Nat. SiO_2 ODC 243 nm	2.202	580 35 265 <15	122	2.1: 1.46033 2.2: 1.46025	67.7	0.18	246/140 290/35 390/120 /166 /35 /170
3 Hera 1	Nat. SiO_2 ODC 243 nm	2.201	2170 1700 500 40	133	3.1: 1.46020 3.2: 1.46016	67.7	0.07	246/75 290/20 390/60 /70 /18 /70
4 SU 300	Synth. Cl′ VUV 170 nm	2.200	<20 20 40 <15 ~1600 ppmw Cl′	0.15 0.06	4.1: 1.460–40 4.2: 1.46035	67.6	<0.01	250/205 280/205 /65 /60
5 SU 312	Synth. VUV 155 nm	nm	nm	246	5.1: 1.46018 5.2: 1.46011	67.8	<0.01	nm
6 SU 2	Synth. VUV 160 nm	2.200	nm	780	6.1: 1.46015 6.2: 1.46006	67.7	<0.01	nm
F1 (800711)	Synth. F′ VUV 150 nm	2.198	F′ ~ 3500 ppmw	0.06	1.45840	67.8	ODC(I) 163 nm ~0.5	nm
F2 (800712)	Synth. F′c VUV 150 nm	2.197	F′ ~ 4300 ppmw	0.06	1.45748	67.9	ODC(I) 163 nm ~0.5	nm

[a]Glass samples from Heraeus Quarzglas GmbH & Co. KG, Hanau, Germany.
nm, not measured. + Intensity I in arbitrary units.

correlation in the absorption and luminescence spectra, but with the same [OH] content (Figure 2C). The ODC(II) in fused silica quartz glass can be made easily visible by illumination with UV light, e.g. with a Hg lamp at 254 nm, providing a strong blue emission (Figure 2D). This can also be used to distinguish between fused quartz and synthetic silica glass samples, which do not show the blue emission under these conditions because they have a not so significant ODC(II) absorption at 243 nm (Figure 3A).

Figure 3A shows the VUV transmission spectra (150–400 nm) of the sample SU 300 (Table 2), which was produced from $SiCl_4$ with Cl treatment (type IIIb) to minimize the OH-content, [OH] ~ 0.1 ppmw. The analyzed Cl-content was 0.16 wt%. An ODC absorption at 243 nm with correlating blue emission could not be recognized under these conditions. However, an absorption at 163 nm and a shift of the absorption edge to 170 nm was found due to the effect of chlorine. The photoluminescence spectra (Figure 3B) provided an excitation band at 250 nm and emission at 260 nm due to the introduction of chlorine. The photoluminescence intensities measured with different samples of one large piece varied between 205 a.u. (sample 4.1) and 65 a.u. (sample 4.2) due to the inhomogeneous distribution of chlorine. The absorption at 163 nm is designated as an ODC(I) [34, 54]. It exists also in the F-containing samples F1 and F2 (Table 2 and Figure 3A),

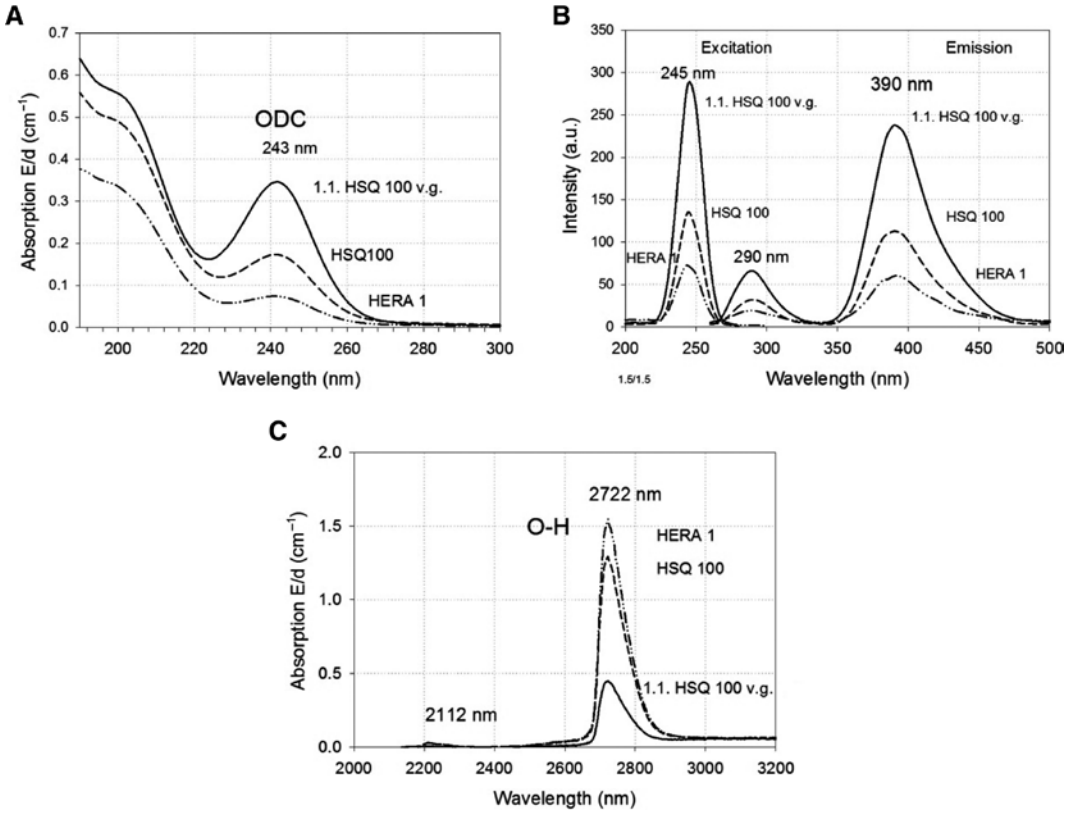

Figure 1: Spectra of various SiO_2 quartz glass types: (A) UV absorption spectra with ODC(II) bands. (B) Photoluminescence excitation (150 W Xe lamp) and emission spectra of the same samples. (C) IR absorption spectra with O-H bands.

which had an analyzed fluorine content, F′ ~ 0.35 wt% and 0.43 wt%. These samples have a very low OH-content, measured by IR absorption [OH] ~0.06 ppmw, but the VUV edge is shifted to a shorter wavelength to λ ~ 150 nm, which is important for applications, e.g. at 157 nm (F_2 laser) for blanks in microlithography and at 172 nm for a Xe discharge lamp [34].

Fluorine incorporation in amorphous SiO_2 by the modified chemical vapor deposition (MCVD) process was studied [55]. The role of fluorine in the structure of silica glass with 3 wt% fluorine was investigated by Youngman [56] with nuclear magnetic resonance (NMR). He found two different environments. Most of the F atoms have replaced one of the bridging oxygens in SiO_4 forming Q^3 species with a ^{19}F chemical shift –146 ppm. Fewer F atoms are bonded additionally to Si with four bridging oxygens forming a fivefold coordination with a ^{19}F chemical shift –137 ppm. Eckert measured already in the year 2002 for the SiO_2-F2 glass sample with 0.5% F′ (Figure 3A) a low ^{19}F-NMR signal with a chemical shift around –150 ppm, which could be caused by the $SiO_{3/2}F$ tetrahedron (it was not published). The refractive indices of the F-doped SiO_2 glass samples are ~$(2–3)\times10^{-3}$ lower than those of un-doped samples. Their densities are also lower (Table 2). The static and time-resolved luminescence of fluorine doped in comparison with non-doped silica glass excited with an ArF laser (193 nm) was studied [57]. Different decay times for the ODC emission was found in the microsecond and millisecond ranges. The thermodynamics of fluorine incorporation into silica glass using different fluorine compounds was calculated [58]. The chemical reaction of molecular dissolved hydrogen with synthetic silica glass (type III) containing various OH contents was investigated between 500°C and 900°C [35]. Hydrogen species H_2, ≡Si—H, and ≡Si—OH play an important role in the defect formation by DUV radiation of high density [33, 34].

3.2 Multicomponent glasses

3.2.1 Fluoride and phosphate glasses

FP glasses based on AlF_3, MF_3 (M = YF_3, LaF_3), $M'F_2$ (M′ = Mg, Ca, Sr, Ba), and P_2O_5 also have a very high intrinsic DUV transmission, complementary to silica glass and fluoride crystals. Investigations of detailed structure-property

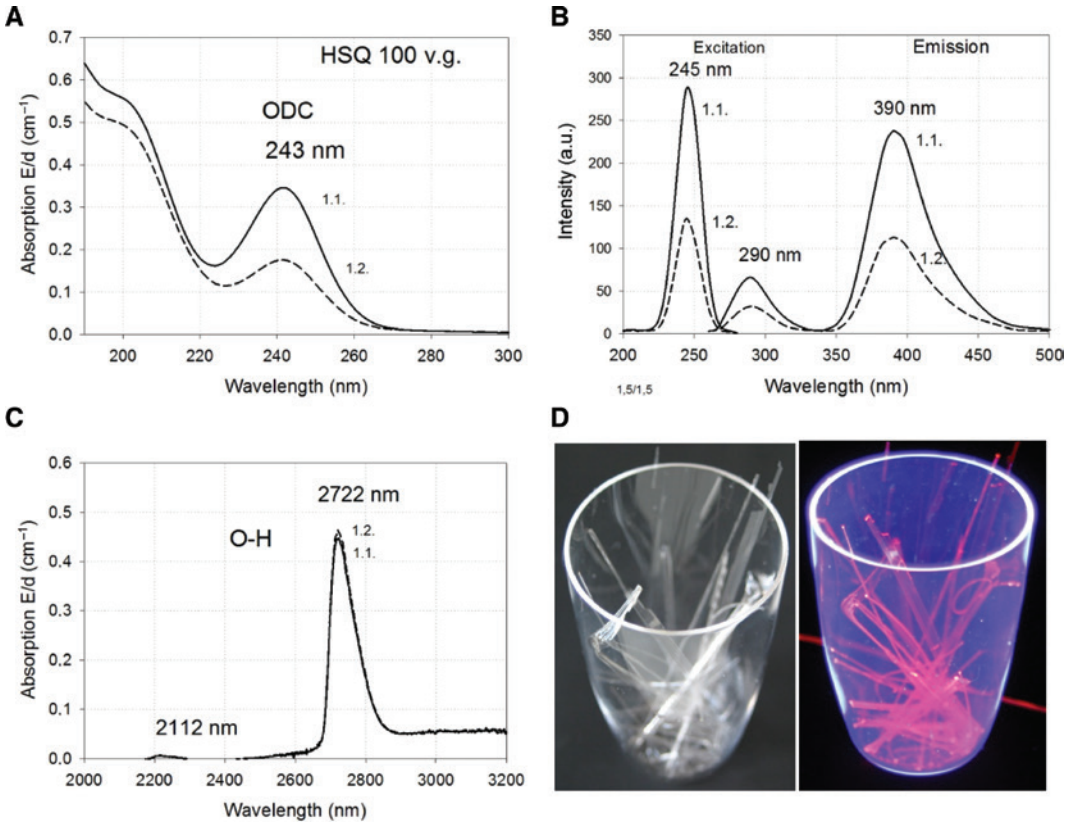

Figure 2: Spectra of ODC(II) (A, B), of O-H (C) of different samples of a large piece of HSQ 100 v.g., and photographs of a silica quartz glass crucible with Eu^{3+}-doped borosilicate glass rods inside (D): crucible and rods are colorless under normal white day light (left), and blue and red under UV light at 254 nm (right) illumination.

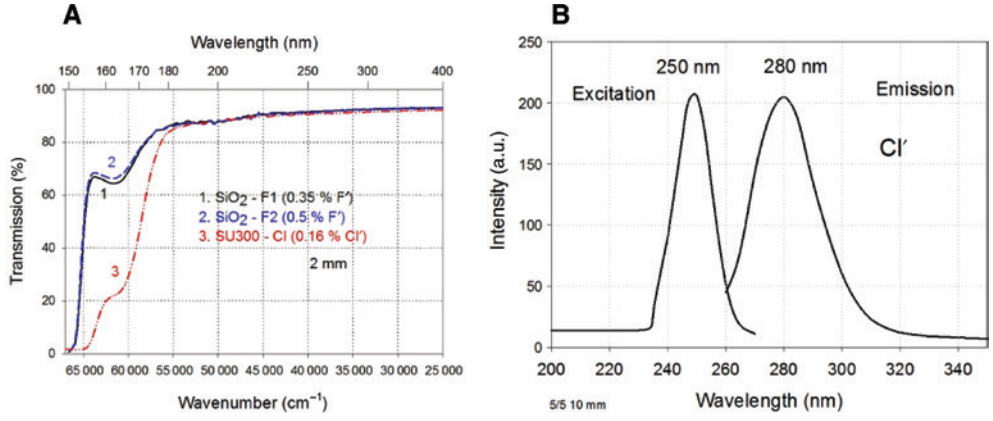

Figure 3: (A) VUV transmission spectra of fluorine (F1 and F2) and chlorine (SU 300) containing SiO_2 glass samples. (B) Photoluminescence spectra of chlorine in SU 300 sample (4.2).

relations of these glasses started at the Otto Schott Institute for Glass Chemistry at the University of Jena, in close collaboration with scientists from JENAer GLASWERK and CARL ZEISS Jena in 1976. The aim was the development of optical glasses with high positive anomalous partial dispersions, making them suitable for lens designs that reduce the secondary spectrum (color distortion) in high-performance optics to substitute CaF_2 single crystals (Figure 4A and B) [2, 5–8]. The crystallization tendency of fluoroaluminate glasses without phosphates is very high due to their strong ionic bonds causing very low viscosity of the melts (Figure 5). Addition of phosphates with higher

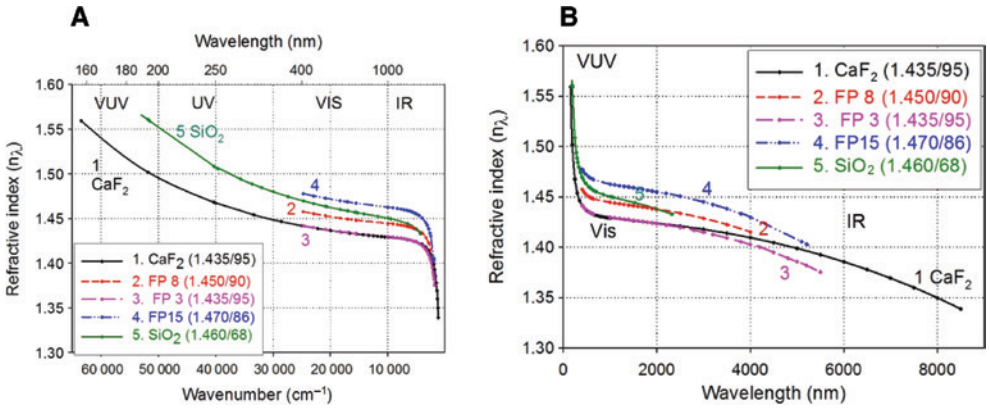

Figure 4: Measured refractive indices for FP glass samples FP3, FP8, and FP15, compared with a commercial SiO_2 glass and commercial CaF_2 single crystals from VUV to IR region: (A) as function of the wave number and (B) as function of the wavelength.

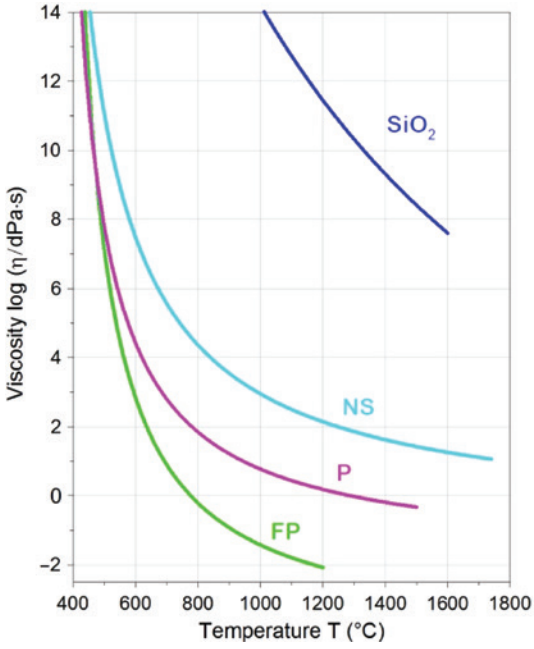

Figure 5: Viscosity curves for different melts of a typical fluoroaluminate glass, FP, a phosphate glass, P, and a silicate glass, NS [12], in comparison with SiO_2 (www.schott.com/lithotec).

covalent bonds decreases the crystallization drastically. The structure model can be described as chains of $Al(F,O)_6$ octahedra, bonding by mono- and diphosphate groups and cations [2, 5]. The intrinsic DUV transmission of FP glasses shifts with increasing P_2O_5 content from ~150 nm (8.2 eV) in FP00 (FA) to ~165 nm (7.5 eV) in FP20 (Table 4), and 180 nm (6.8 eV) in pure metaphosphate, $Sr(PO_3)_2$. However, the real DUV transmission is limited by trace impurities, mainly transition metal ions in different redox states, introduced by the impurities of raw materials and contact with container materials for the melts. The absorption coefficients of possible trace impurities in different redox states were determined. The properties, structure, and applications of these optical glasses, the so-called FP, commercially fluor crown (FC, or in German FPSK, FK), are summarized in a review paper [7].

The measured dispersion curves from VUV (DUV) to IR of CaF_2 single crystal and amorphous SiO_2 [SCHOTT Lithotec Jena (www.schott.com/lithotec)] are compared with three FP glass samples with increasing P_2O_5 content of 3 (FP3), 8 (FP8), and 15 (FP15) mol% as a function of energy in Figure 4A and as a function of wavelength in Figure 4B. The values for the refractive index n_e and dispersion coefficient (Abbe number) ν_e are given inside the figures. The values of refractive indices increase with increasing phosphate content, and the dispersion coefficients decrease. The glass FP3 has identical dispersion to CaF_2 from the visible to the near-infrared region (NIR) region (~3000 nm). The stronger decrease in the IR is due to the P—O overtone and combination vibrations, which increase with increasing phosphate content [7]. The OH content of FP glasses is very low. The absorption (or extinction) coefficient at $\lambda \sim 3000$ nm is <0.1 cm^{-1} (OH <3 ppm), which has no significant effect on the dispersion curves.

The T_g values for the three glasses, FP, P, and NS, are very similar, but the viscosity values at higher temperatures are very different. FP melts have extreme viscosity behavior due to their strong ionic bonds. The viscosity is at 1200°C comparable with water at room temperature, $\eta \sim 0.01$ dPa s, and increases rapidly at $T < 700$°C. The viscosity values of the more covalent phosphate and silicate melts are much higher; however, the silica melts have extremely higher viscosity, with $T_g > 1000$°C, and softening point (log $\eta = 7.6$ dPa s) $T \sim 1600$°C, due to different structures.

Glass melts with lower viscosity than SiO_2 usually have a high solubility for trace impurities, e.g. polyvalent metal ions, which limit the DUV transmission due to

high absorption of allowed charge transfer, s→p, or d→s transitions of electrons with very high intensity. They are very sensitive to the surrounding matrix depending on the 'optical basicity' (electron donor power) of the glasses (Table 3). Fe′ ions, such as Fe^{3+} and Fe^{2+}, are the most common impurity in the range from 1 to 200 ppm in multicomponent glasses, which mostly limit the DUV transmission.

Figures 6A,B and 7A,B demonstrate the effect of different ions on the DUV absorption and transmission of FP glasses. High-purity FP10 glasses with a DUV edge at ~160 nm (Figure 5B), doped with different ions in the ppm range, were prepared under various conditions to obtain the ions in different redox states. This was intensively studied and published in former papers [2, 6, 7, 10, 11, 14, 15]. Ag^+, with $3d^{10}$ electronic configuration, has an absorption maximum at 213 nm (Figure 5A) due to d→s transition with a specific absorption coefficient, $\varepsilon_{213\,nm} \sim 0.1\ cm^{-1}\ ppmw^{-1}$. Ti^{4+}, with a $3d^0$ electronic configuration, causes a charge transfer transition with an absorption maximum at 225 nm (Figure 5B) with a specific absorption coefficient, $\varepsilon_{225\,nm} \sim 0.5\ cm^{-1}\ ppmw^{-1}$. Both ions also provide a photoluminescence emission, Ag^+ in the UV at ~350 nm, and Ti^{4+} in the visible (green) at ~500 nm, after excitation in the absorption bands [12, 15].

Cu^{2+} with electronic configuration $3d^9$ and Cu^+ with $3d^{10}$ generates strong absorption bands in the DUV (Figure 7A and B) by the allowed d→s electron transitions leading to a strong decrease in the DUV transmission. The absorption coefficient of Cu^{2+} around 250 nm, $\varepsilon_{230\,nm} \sim 0.1\ cm^{-1}\ ppm^{-1}$, is much higher than the absorption coefficient of Cu^+, $\varepsilon_{240\,nm} \sim 0.04\ cm^{-1}\ ppm^{-1}$ (Figure 7A). However, both ions have additionally strong absorption bands in the VUV, with maxima at ~180 nm. These absorption coefficients were determined for Cu^{2+} $\varepsilon_{180\,nm} \sim 0.2\ cm^{-1}\ ppm^{-1}$, and a much higher value for Cu^+ with $\varepsilon_{180\,nm} \sim 0.4\ cm^{-1}\ ppm^{-1}$ [2, 6, 7, 11]. The effect of oxidizing and reducing melting conditions was studied using a Pt crucible in air atmosphere, and a carbon crucible with argon as a protective gas to avoid the oxidizing of the carbon crucible. Bi^{3+} ions with the electronic configuration $6s^2$ possess allowed s→p transitions, which are comparable with the s→p transitions of Pb^{2+} ions, which have also $6s^2$ electronic configuration. The absorption bands of the s→p transitions are very sensitive to the surrounding glass matrix and can be used to determine the optical basicity of the glasses. The absorption coefficient, ε, for Bi^{3+} at 219 nm is ~0.1 $cm^{-1}\ ppm^{-1}$. The FP10 glass sample doped with 50 ppm Bi^{3+}, melted under reducing conditions in a carbon crucible, has a much lower absorption at ~220 nm (Figure 7B). Only ~10 ppm Bi^{3+} can be calculated. It should be assumed that Bi^{3+} can be reduced to a lower species, e.g. Bi^{2+}, with another absorption behavior [48].

3.2.2 Borosilicate glasses

Borosilicate glasses with different compositions are very important for applications such as technical and optical glasses. During the second half of the 19th century, Otto Schott, working with Ernst Abbe and Carl Zeiss in Jena, performed seminal results. This early research was of great significance because it represented a first attempt to study systematically the relationships between the composition of a glass and its physical and chemical properties. The introduction of B_2O_3 allowed a minimization of the 'secondary spectrum' and a better achromatization for telescope and microscope objectives, on the one hand, and, on the other, a large-scale production of technical borosilicate glasses with high thermal, chemical, and mechanical resistance [26]. The structure and properties of borosilicate glasses are mainly determined by the $(M_2, M')O/B_2O_3$ and the B_2O_3/SiO_2 ratio. We prepared and investigated in my research group many different borosilicate glasses over a long period [13–16, 26, 27, 41–44, 46, 48–50]. Two traditional borosilicate glass types, the well-known optical glass BK7 with high alkali/alkaline earth content, and the technical glass Duran® (similar to Pyrex® [51, 52]) with low alkali oxide and very high SiO_2 content were melted with starting materials of special high purity (Fe′ < 1 ppm). It was found that they had different DUV transmission depending on nonbridging oxygen (NBO) content. BK7 with higher NBO content has a lower intrinsic bandgap, ~6.3 eV, and an intrinsic UV edge at ~195 nm. Duran® composition leads to nearly only bridging oxygen (due to the so-called boric oxide anomaly) with an extreme intrinsic UV edge ~175 nm and a very low thermal expansion coefficient, TEC $\sim 3 \times 10^{-7}$/K [26, 27]. Borofloat® is commercially produced with Duran® composition by floating on an Sn bath [45]. Figure 8A shows the effect of 20 ppmw Fe′ as Fe^{3+} and Fe^{2+} on the DUV transmission of high-purity Duran glass samples. Figure 8B demonstrates the DUV transmission loss in Duran glass samples with a different impurity level of Fe′ 1, 20, 100, and 200 ppmw (doped as Fe′ ions and melted under reducing conditions) [14].

Commercial Borofloat® samples with high transmission in the UV-B region (280–320 nm) due to a relatively low impurity content (for a technical glass) was investigated. Figure 8C shows a commercial Borofloat® sample with Gaussian band simulation for Fe^{3+} and Ti^{4+} in comparison with the values determined by chemical analysis. TiO_2 (introduced with the raw material SiO_2), 56 ppm, was

Table 3: Overview on values for theoretical and measured optical basicity and measured properties of various glasses.

Glasses	Pb^{2+} absorption with fit			Absorpt. coeff. $\varepsilon_{Pb^{2+}}$	Pb^{2+}-PL Excit./Em.	Opt. basicity		Refract./ Abbe number n_e/ν_e	Density
Composition in mol%	Max. (±1 nm)	Max. (cm^{-1})	HWHM (cm^{-1})	(ppm^{-1} cm^{-1})	(±3 nm)	Λ_{th} (±0.01)	Λ_{Pb} (±0.01)	$\Delta n \pm 2 \times 10^{-5}$	(±0.01 g/cm^3)
AF: $2BaO\text{-}9CaO\text{-}4MgO\text{-}10Al_2O_3\text{-}8B_2O_3\text{-}67SiO_2$	230	43 500	5600	0.06	280/350	0.53	0.56	1.5230/62	2.56
BC: $10BaO\text{-}10CaO\text{-}15Al_2O_3\text{-}65SiO_2$	234	42 700	5500	0.06	280/365	0.57	0.58	1.5560/60	2.85
BBC: $5BaO\text{-}10CaO\text{-}10Al_2O_3\text{-}10B_2O_3\text{-}65SiO_2$	231	43 200	5400	0.05	275/360	0.57	0.56	1.5360/61	2.57
BK7: $\sim 15Na_2O/K_2O\text{-}1BaO\text{-}10B_2O_3\text{-}74SiO_2$	232	43 100	4600	0.06	265/375	0.55	0.56	1.5115/65	2.53
NBS1: $10Na_2O\text{-}10B_2O_3\text{-}74SiO_2$	230	43 500	5100	0.07	250/380	0.55	0.56	1.5109/63	2.45
NBS2: $\sim 4Na_2O\text{-}1Al_2O_3\text{-}21B_2O_3\text{-}74SiO_2$	222	45 100	4900	0.05	260/350	0.49	0.50	1.4706/65	2.17
Duran: $\sim 5Na_2O/K_2O\text{-}1Al_2O_3\text{-}12B_2O_3\text{-}82SiO_2$	233	42 900	7000	0.02	275/390+430	0.48	0.58	1.4725/66	2.22
NBS-A: $12.5Na_2O\text{-}62.5B_2O_3\text{-}25SiO_2$	217	46 100	5600	0.07	nm	0.47	0.47	1.4962/62	2.18
NBS-B: $3Na_2O\text{-}48.5B_2O_3\text{-}48.5SiO_2$	213	46 900	5000	0.10	nm	0.45	0.44	1.4715/62	2.04
NBS-C: $15Na_2O\text{-}42.5B_2O_3\text{-}42.5SiO_2$	225	44 500	6500	0.05	260/370	0.49	0.52	1.5063/64	2.31
NBS-D: $6.5Na_2O\text{-}33.5B_2O_3\text{-}60SiO_2$	218	45 800	5400	0.06	260/335	0.47	0.48	1.4760/64	2.15
NS15: $15Na_2O\text{-}85SiO_2$	228	43 900	3800	0.06	260/370	0.53	0.54	1.4833/61	2.34
NS33: $33Na_2O\text{-}67SiO_2$	231	43 300	4500	0.07	260/370	0.61	0.56	1.5083/55	2.49
NCS: $16Na_2O\text{-}10CaO\text{-}74SiO_2$	229	43 700	4700	0.06	265/375	0.57	0.54	1.53/60	2.49
NSP: $10Na_2O\text{-}40SrO\text{-}50P_2O_5$	216	46 300	4500	0.12	243/310	P_2O_5 0.33 0.46	0.46	1.5468/65	3.05
SP=P100: $50SrO\text{-}50P_2O_5$	216	46 300	4500	0.12	245/310	0.455[a]	0.465[a]	1.5589/66	3.20
MgP: $50MgO\text{-}50P_2O_5$	214	46 800	5400	0.08	245/300	0.41	0.45	1.4988/70	2.43
ZnP: $50ZnO\text{-}50P_2O_5$	213	47 000	4700	0.2	245/315	0.43	0.44	1.5262/61	2.88
CaP: $50CaO\text{-}50P_2O_5$	216	46 300	4800	0.10	245/320	0.44	0.46	1.5491/66	2.65
BaP: $50BaO\text{-}50P_2O_5$	219	45 600	5100	0.12	265?/330	0.47	0.49	1.5907/64	3.66
AlP: $25Al_2O_3\text{-}75P_2O_5$	212	47 100	5500	0.10	245/310	0.38	0.44	1.5310/70	2.60
NaP: $NaPO_3$	220	45 500	4300	0.11	-	0.47	0.49	1.4869/65	2.51
NaPAF-20: $80NaPO_3\text{-}20AlF_3$	216	46 300	4500	0.11	240/315	0.44	0.47	1.4722/71	2.63
NaPAF-30: $70NaPO_3\text{-}30AlF_3$	214	46 700	4700	0.11	240 / 305	0.43	0.45	1.4689/73	2.71
FP02: $98(AlF_3\text{-}MF_2)\text{-}2P_2O_5$	194	51 700	7500	0.09	nm	0.317[a]	0.290[a]	1.4210/98	3.44
FP04: $96(AlF_3\text{-}MF_2)\text{-}4P_2O_5$	200	50 000	6700	0.10	225/295	0.322[a]	0.345[a]	1.4350/94	3.46
FP10: $90(AlF_3\text{-}MF_2)\text{-}10P_2O_5$	206	48 500	4800	0.10	230/300	0.339[a]	0.394[a]	1.4567/90	3.43
FP20: $80(AlF_3\text{-}MF_2)\text{-}20P_2O_5$	212	47 200	4700	0.11	230/300	0.366[a]	0.436[a]	1.5045/80	3.52
FP30: $70(AlF_3\text{-}MF_2)\text{-}30P_2O_5$	216	46 300	5600	0.13	245/320	0.386[a]	0.463[a]	1.5401/73	3.51

*Ref. [19].

nm, not measurable.

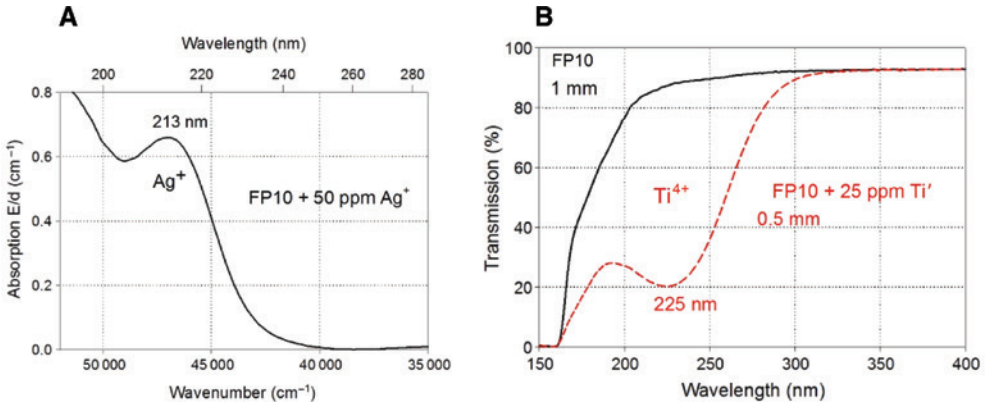

Figure 6: Effect of 50 ppmw Ag^{+}-doped FP10 glass on normalized DUV absorption (A) and effect of 25 ppmw Ti^{4+}-doped FP10 glass (B).

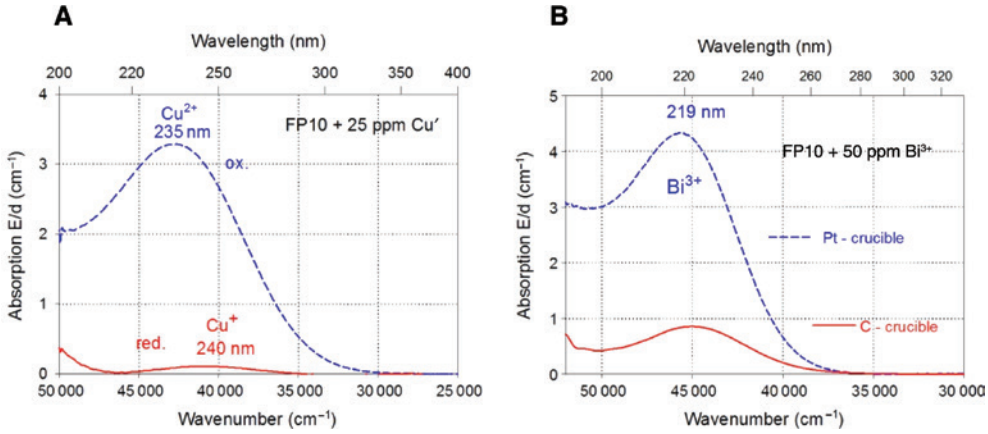

Figure 7: Effect of 25 ppmw Cu^{2+} and Cu^{+} (A) and 50 ppmw Bi^{3+}, oxidizing melted in a Pt crucible and reducing in a carbon crucible (B), on the DUV absorption of FP10 glass samples.

determined by band simulation with $\varepsilon_{201\,nm} = 0.3\,cm^{-1}\,ppm^{-1}$. This is in very good agreement with the value of 55 ppm of the chemical analysis. The total Fe′ content determined by chemical analysis was 95 ppm. By band simulation, 67 ppm Fe^{3+} was calculated with $\varepsilon_{222\,nm} = 0.3\,cm^{-1}\,ppm^{-1}$. The difference of 28 ppm should be Fe^{2+}. It has a very low value of the absorption coefficient at 215 nm ~ 0.03 cm^{-1} ppm[1] [14]. We can, therefore, deduce that it is not possible to detect Fe^{2+} besides high Fe^{3+} content by band simulation in the DUV [44].

Cu^{+} ($3d^{10}$) and Cu^{2+} ($3d^{9}$) ions also have, in borosilicate glasses, a strong absorption in the DUV region and can cause different effects depending on the redox states of the preparation process, which is shown in Figure 9A–D. High-purity Duran® glass samples doped with 38, 380, and 3800 ppm Cu′ were melted under normal conditions and under reducing conditions. The samples have different colors under daylight illumination (Figure 9A and B). The green coloring is due to a broad absorption band from d→d electron transitions of Cu^{2+} with a maximum at ~800 nm. Glasses melted under reducing conditions (addition of 0.5 wt% sugar as reducing agent) show a red color (copper ruby glass) with 38 and 380 ppm Cu′ due to the absorption of Cu^{0} (broad band between 300 and 400 nm) and Cu_2O (small band at ~570 nm) colloids. Cu^{+} is known for blue photoluminescence emission by UV excitation in different glasses [7], which is mainly dependent on Cu^{+} content, filter effect from Cu^{2+}, or other UV-absorbing species limiting the Cu^{+} excitation (Figure 9C and D).

CeO_2 doping in glasses is used for different applications. Ce^{3+} with an electronic configuration $4f^{1}$ causes f→f and Ce^{4+} ($4f^{0}$) f→d transitions of electrons, which absorb in the DUV region (Figure 10A) [9]. This is used as effective protection against UV radiation, e.g. in special silica glasses. Furthermore, the existence of Ce^{3+} and Ce^{4+} concurrently is an effective protection against the formation of radiation-induced color centers in the visible region. Under UV or X-ray radiation, Ce^{3+} loses an electron forming a $(Ce^{3+})^{+}$ hole center, and Ce^{4+} accepts the electron forming

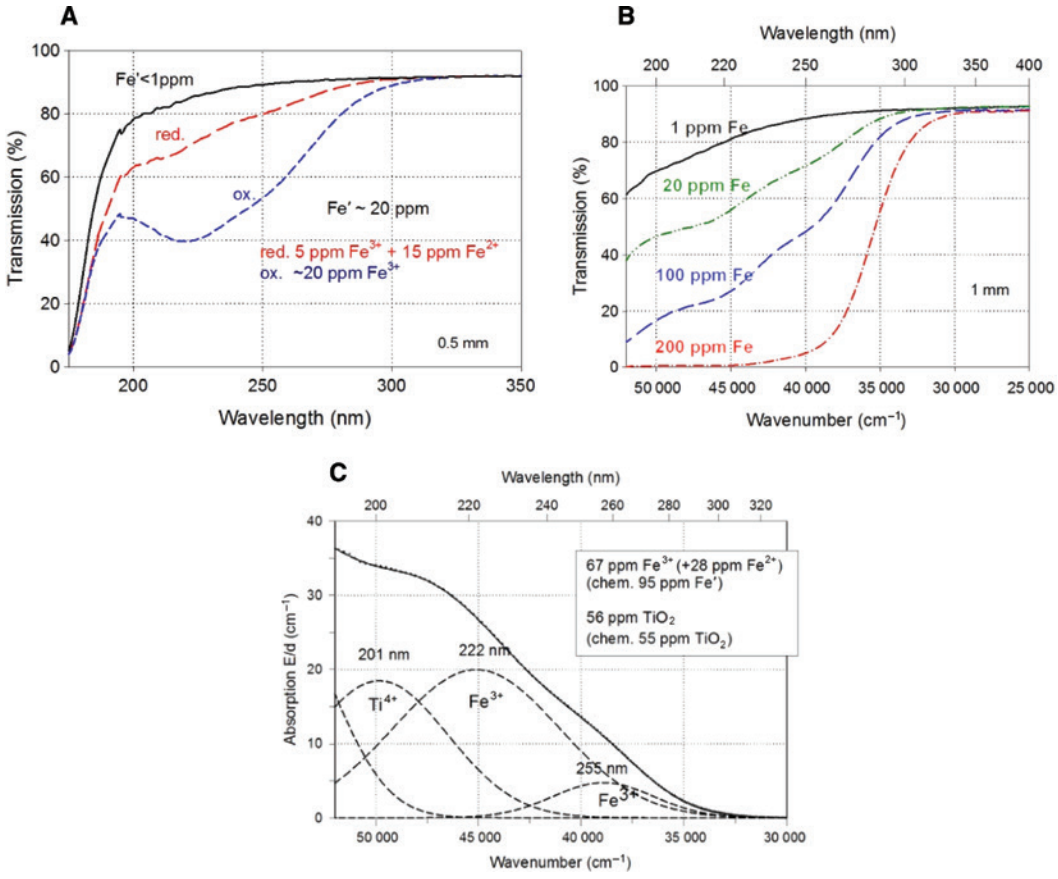

Figure 8: Effect of impurities in the DUV region: (A) DUV transmission of Duran® glass samples with Fe′ < 1 ppm and 20 ppm melted under oxidizing and reducing conditions. (B) DUV transmission of Duran® samples with increasing Fe′ content from ~1 to 200 ppm melted under reducing conditions. (C) Gaussian band simulation for Fe^{3+} and Ti^{4+} of a commercial Borofloat® glass sample [44].

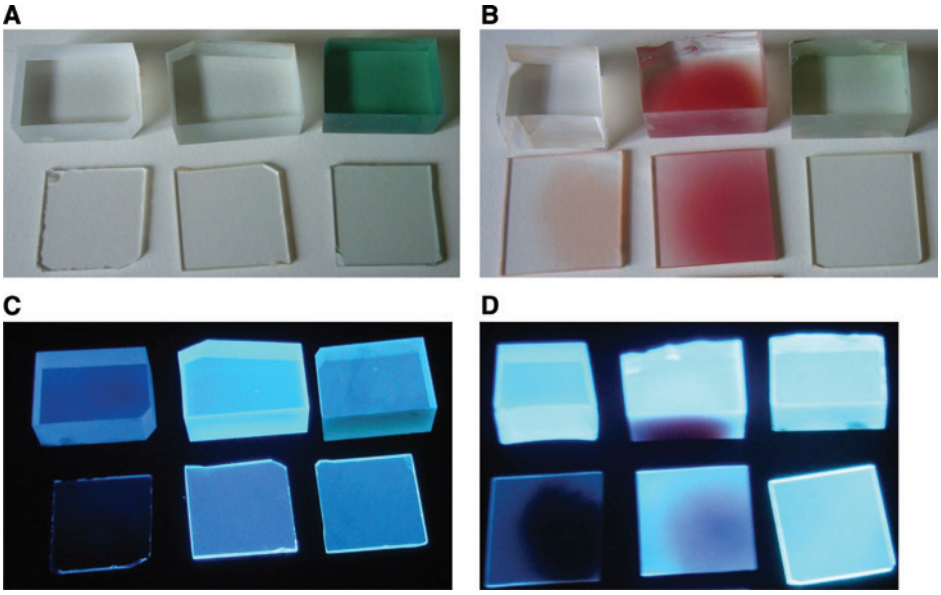

Figure 9: Duran samples (thickness 10 and 1 mm) doped with increasing Cu′ content, 38, 380, and 3800 ppm: (A) Melted under normal conditions at 1650°C in silica glass crucible (photo under normal daylight). (B) Melted under reducing conditions by addition of 0.5 wt% sugar at 1650°C (photo under normal daylight). (C) Samples from (A) under UV light (Hg lamp 254 nm) with blue emission of Cu^{+}. (D) Samples from (B) under UV light (Hg lamp 254 nm) with blue emission of Cu^{+}.

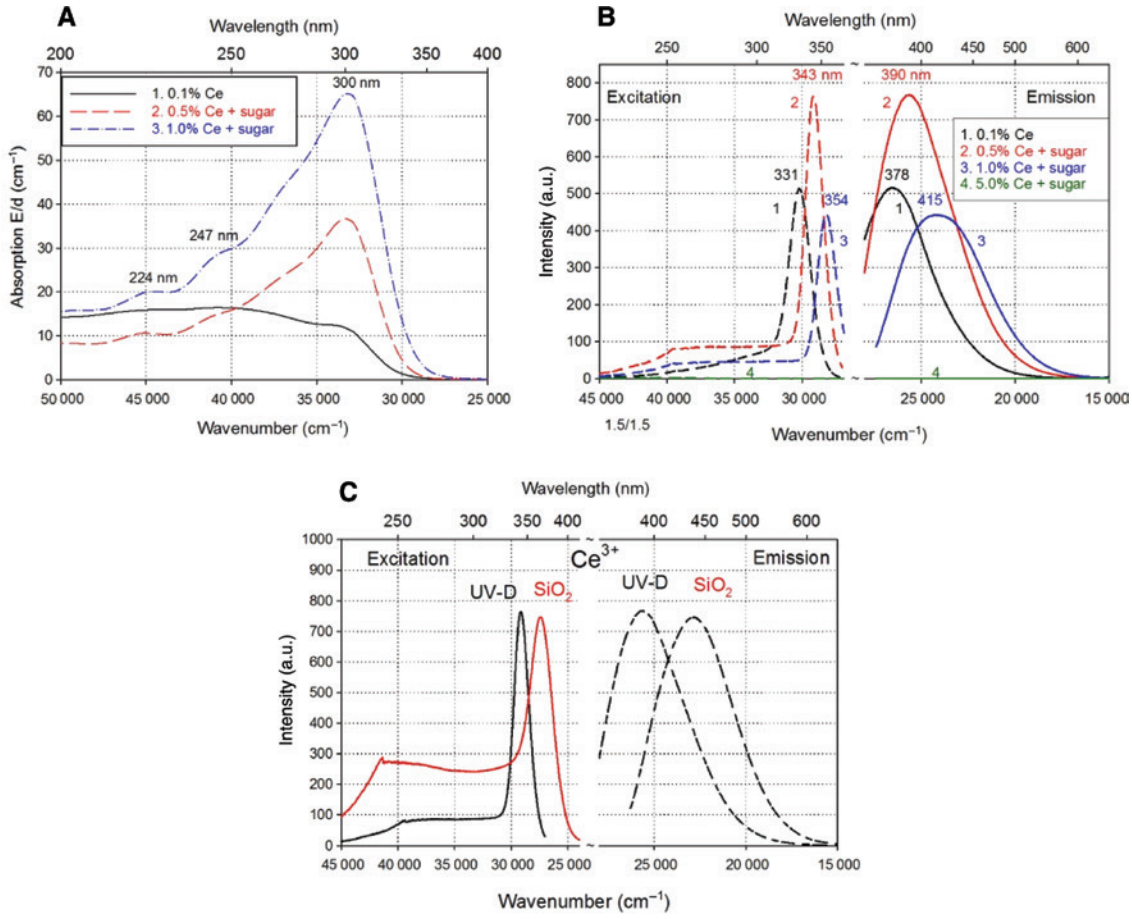

Figure 10: Effect of Ce^{3+} and Ce^{4+} on Duran and SiO_2 glass samples: (A) DUV absorption of Ce^{3+} and Ce^{4+} in UV-Duran® doped with 0.1 wt% Ce′, 0.5 and 1.0 wt% Ce′ + sugar as reducing agent. (B) Photoluminescence excitation and emission spectra of Ce^{3+} in UV-Duran® glasses with different Ce′ content, 0.1–5.0 wt%. (C) Photoluminescence spectra of Ce^{3+} in UV-Duran® and SiO_2 glass samples.

a $(Ce^{4+})^-$ electron center. Both color centers absorb only in the UV and not in the visible region. Only Ce^{3+} ions show a blue emission (Figure 10B and C). Ce^{3+}-containing glasses are also used as scintillator glass.

4 Optical basicity of glasses

The concept of optical basicity was developed as a general method for quantifying variations in Lewis basicity in a wide range of compositions. Optical basicity of glasses is applied to express the electron donor power of a host matrix by the theoretical (ideal) basicity, Λ_{th} and the experimentally determined optical basicity, Λ_{ex}. The last could be determined using suitable probe ions, mostly with s^2 electronic configurations such as Pb^{2+}. The experimental optical basicity, $\Lambda_{Pb}{}^{2+}$, is calculated by measuring the red shift of the characteristic $^1S_0 \rightarrow {}^3P_1$ electronic transition of the Pb^{2+} probe ion. Pioneering papers were published by Duffy & Ingram starting already in 1971 [17, 18]. We investigated the theoretical and measured optical basicity of different glasses by melting with high purity and doping with Pb^{2+} ions, 50 to 200 ppm [6, 7, 10, 13–15, 19] and measured the Pb^{2+} absorption and luminescence. Typical spectra are shown in Figure 11A–C. An overview of the data of all the investigated glasses is given in Table 3. Additionally, the values for specific absorption coefficient, $\varepsilon_{Pb}{}^{2+}$, in different glasses, for refractive index, Abbe number, and density are determined to characterize the different glass samples. Figure 11A shows the red shift of the Pb^{2+} absorption maximum for FP glass samples doped with 50 ppm Pb^{2+} with increasing phosphate content, 4, 10, and 20 mol%, according to 200, 206, and 212 nm, due to increasing optical basicity, $\Lambda_{Pb}{}^{2+}$ 0.34, 0.39, and 0.44 (Table 3). Figure 11B demonstrates the influence of cations in metaphosphate glass samples. The red shift of Pb^{2+} absorption maximum increases with increasing ionic radius of the cation. That means that the optical basicity, $\Lambda_{Pb}{}^{2+}$, increases in the

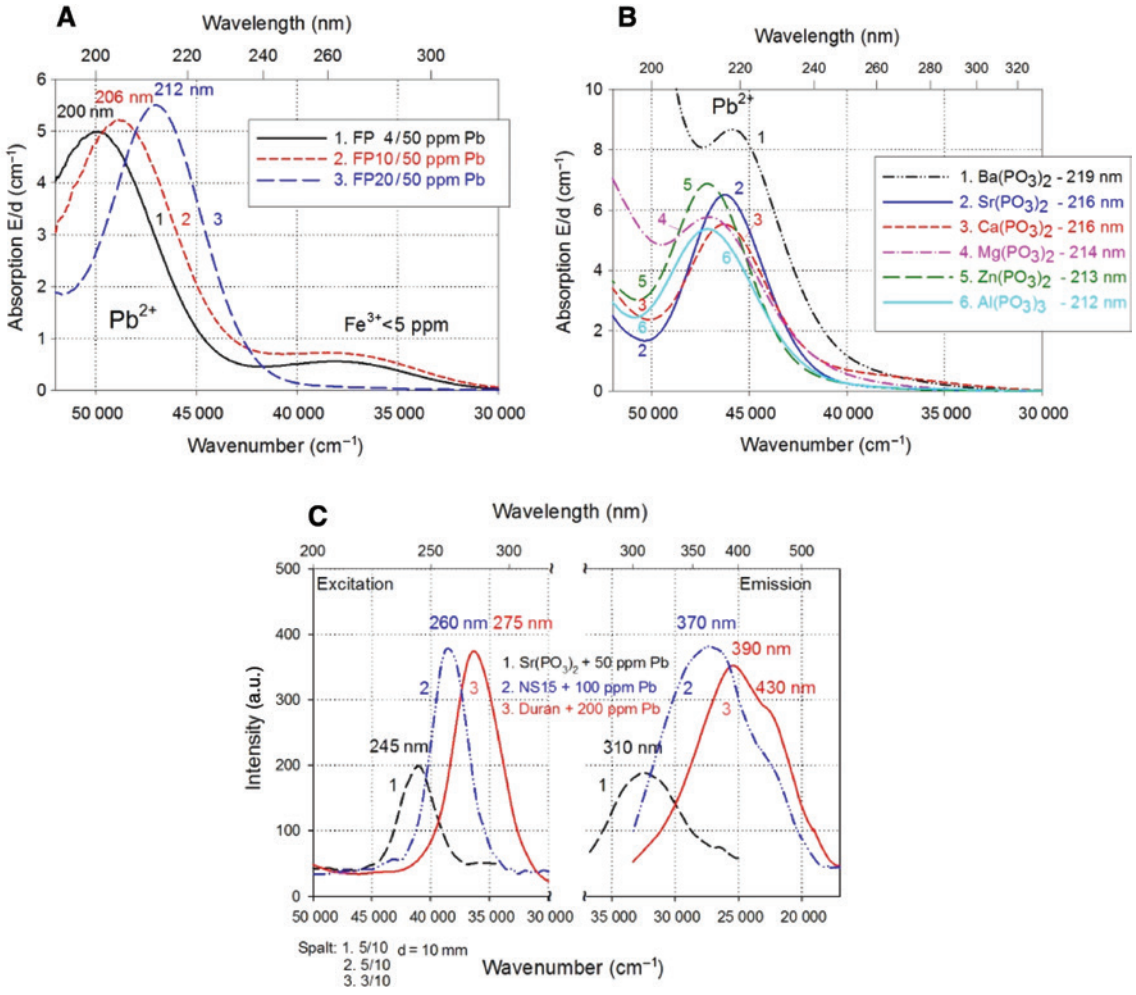

Figure 11: Pb^{2+} as probe ion in various glasses: (A) Absorption in FP glass samples. (B) Absorption in metaphosphate glasses. (C) Photoluminescence excitation and emission in phosphate, sodium silicate NS15, and Duran®.

Table 4: Overview on measured properties of different glasses.

Glass	Refract. index n_e	Abbe number ν_e	UV edge λo (nm)	$1/\lambda_o$ (cm^{-1})	Gap (eV)
CaF_2 crystal	1.435	95	~125	80 000	10.0
SiO_2	1.460	68	~150	66 700	8.2
FA00	1.405	105	~150	66 700	8.5
FP04	1.435	95	~155	64 500	8.0
FP10	1.460	90	~160	62 500	7.8
FP20	1.504	80	~165	60 600	7.5
$DURAN_s$	1.473	66	~175	57 100	7.0
Phosphate $65P_2O_5$-31MO-$4Al_2O_3$	1.540	67	~185	54 000	6.7
$BK7_s$	1.515	64	~195	51 200	6.3
NaCa-$silicate_s$ $16Na_2O$-10CaO-$74SiO_2$	1.520	60	~198	50 500	6.2
F-$silicate_s$ (FK5) $66SiO_2$-$15B_2O_3$-$12K_2O$-7KF	1.490	70	~190	52 600	6.5
Pb-$silicate_s$ (LF5) $72SiO_2$-$15(K,Na)_2O$-13PbO	1.583	41	~290	34 500	4.3
Bi-$borate_s$ $73Bi_2O_3$-$27B_2O_3$	2.298	15	~400	25 000	2.0

range $Al(PO_3)_3 < Zn(PO_3)_2 < Mg(PO_3)_2 < Ca(PO_3)_2 \approx Sr(PO_3)_2 < Ba(PO_3)_2$. However, larger differences between theoretical, Λ_{th}, which is an average value, and measured, $\Lambda_{Pb^{2+}}$, values were found for $Al(PO_3)_3$ and $Mg(PO_3)$ (Table 3). The values for the measured optical basicity, $\Lambda_{Pb^{2+}}$, are strongly dependent on the local site (environment) of the probe ion Pb^{2+} [17, 18]. Larger deviations were also found in glasses FP02, FP20, and FP30 (Table 3) in agreement with structural evidence [19]. The lowest values, $\Lambda_{Pb^{2+}} = 0.265$ and $\Lambda_{th} = 0.309$, were determined for the pure fluoroaluminate glass (FA = FP00), which has the lowest intrinsic UV edge, $\lambda_0 \sim 150$ nm, comparable with amorphous SiO_2 and near the CaF_2 single crystal (Table 4). For SiO_2 glass with only bridging oxygen in the structure, a theoretical optical basicity, $\Lambda_{th} = 0.48$, is given by Duffy & Ingram [17]. With the addition of Na_2O, nonbridging oxygens are formed with higher electron donor power. Optical basicity, $\Lambda_{Pb^{2+}} = 0.54$ for NS15, and $\Lambda_{Pb^{2+}} = 0.56$ for NS33 (Table 3) were determined.

The lowest value for the optical basicity of multicomponent silicate glasses (Table 3) was found with $\Lambda_{Pb^{2+}} = 0.44$ in a borosilicate glass NBS-B with only 3 mol% Na_2O. The value increases to $\Lambda_{Pb^{2+}} = 0.48$ in NBS-D with 6.5 mol% Na_2O and to $\Lambda_{Pb^{2+}} = 0.52$ in NBS-C with 15 mol% Na_2O [59]. The highest value, $\Lambda_{Pb^{2+}} = 0.58$, was found for alkali-free alkaline earth aluminosilicate glass BC [47] and, surprisingly, for Duran® with a large deviation from the theoretical value, $\Lambda_{th} = 0.48$ [60]. The reason should be the existence of special local sites for the large Pb^{2+} ion in the Duran® structure, which should mainly possess bridging oxygens connecting $Si\,Ø_4$, $B\,Ø_4^-$, and $B\,Ø_3$ groups. This causes the high intrinsic DUV transmission [13, 14, 26, 27, 41–44, 49–52]. The ternary system Na_2O-B_2O_3-SiO_2 has a subliquidus immiscibility gap. This leads to cluster formation and phase separation [59–63]. The Pb^{2+} probe ions could form clusters in low alkali borosilicate glasses, too, as shown in the cases of Eu′ and Mn^{2+} ions.

Table 4 gives an overview of the measured optical properties, n_e and ν_e, intrinsic UV edge, and bandgap. Oxide glasses with only bridging oxygens, SiO_2 and Duran®, have a low intrinsic UV edge λ_0 and a high bandgap. The UV edge increases with the nonbridging oxygens (BK7, NaCa-silicate). Fluorine in oxide glasses (FK5) decreases the UV edge and the refractive index. The bandgap of fluoroaluminate glasses FP decreases with increasing phosphate content, FA = FP00, FP04, FP10, FP20. The introduction of PbO and Bi_2O_3 increases the refractive index and decreases the bandgap due to the red shift of the UV edge by s→p electron transition of Pb^{2+} and Bi^{3+} [26, 64].

5 Radiation damage

Radiation damage of optical materials is a very important property in determining their suitable applications. The demand for special glasses with high UV transmission and high radiation resistance has increased in the same way as the use of UV radiation by sunlight, lamps, and lasers. Both the UV transmission and the UV radiation resistance of glasses can be correlated with the optical basicity of the glass matrix as intrinsic effects and the possible trace impurities as extrinsic effects. Synthetic CaF_2 single crystals are produced commercially in very high quality and are a key material in the 193-nm microlithography and laser applications. They have excellent damage behavior without compaction and rarefaction effects known from synthetic fused silica [30–32]. Radiation damage behavior of synthetic fused silica of different types was extensively investigated [33, 34, 36–40, 54]. It was found that ODC(I), ODC(II), SiOH, SiH, SiCl, and H_2 play an important role. They can act as precursors for generation of defects, E′ center, absorbing at 215 nm, NBOH centers, absorbing at 265 nm and emitting red fluorescence at 650 nm under laser excitation (LIF) by two-photon absorption and additional one-photon absorption. Synthetic fused silica of types III and IIIa with different OH and molecular H_2 content were prepared and irradiated with tens of billions of 193-nm laser pulses of low energy densities below 50 μJ/cm³. Compaction and rarefaction effects were observed depending on OH and H_2 content [40]. However, the radiation damage of synthetic SiO_2 glasses, which can be manufactured with extremely high purity from $SiCl_4$, available with extremely high purity, too, is very low in comparison with multicomponent glasses. The reason is the special structure of SiO_2. Pure AlF_3-based fluoride glasses have the largest intrinsic UV transmission and the largest UV radiation resistance. By increasing phosphate content, the intrinsic UV transmission and radiation resistance decrease. The unavoidable main polyvalent trace impurities affecting UV absorption and radiation effects are Fe^{3+}/Fe^{2+}, Cu^{2+}/Cu^{+}, $P^{5+}/P^{3+}/P^0$, etc. Fe^{2+} causes UV absorption around 250 nm, which is lower than Fe^{3+} in all glasses investigated. Therefore, reducing melting conditions are often used to obtain glasses with higher UV transmission [2, 5–14]. However, Fe^{2+} is photoionized by a single-photon mechanism forming stable $(Fe^{2+})^+$ hole center (HC) and electron center (EC) defect. The defect rate depends mainly on the optical basicity of the glass matrix. Only phosphorous-related intrinsic radiation-induced defects were found in FP and P glasses. Phosphorous-related hole centers (POHC) absorb in the visible range (~400 to 600 nm) turning the glasses brown.

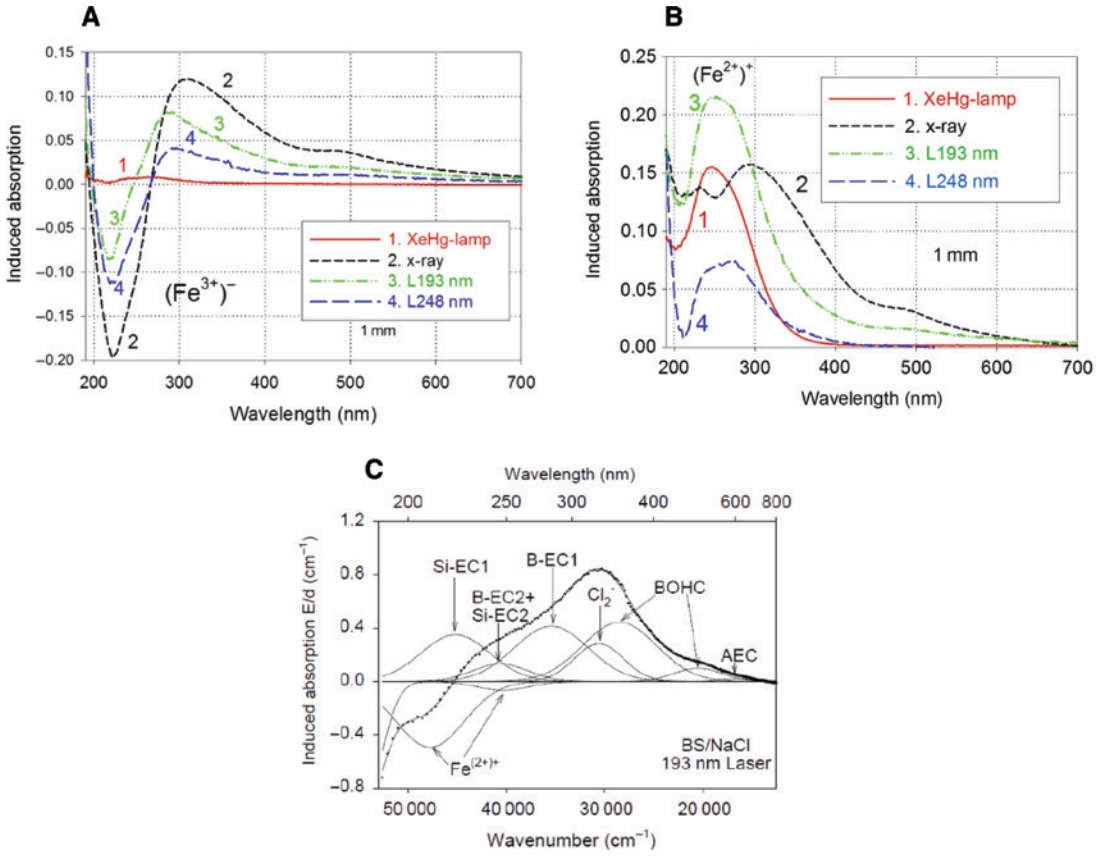

Figure 12: Radiation-induced defect formation in high-purity borosilicate glass samples: (A) Duran with 20 ppm Fe, oxidized melted, radiated with different sources. (B) Duran with 20 ppm Fe reduced melted. (C) Borosilicate glass sample (SCHOTT 8337B) with NaCl as refining agents, irradiated with 193 nm laser, and band simulation by fitting with Gaussian bands.

This color could be removed by thermal treatment below T_g (100–300°C) or by other radiation. Fe^{2+} and P^{3+} suppress the formation of intrinsic POHC in FP and P glasses [10, 20–25]. We have studied the generation of defects induced by different irradiation (X-ray, UV lamps, and UV lasers) in silicate and borosilicate glasses without and with doping of polyvalent ions [26–29, 41–44, 65, 66].

The redox states, especially of Fe^{3+} and Fe^{2+}, and the radiation sources play an important role. This is shown in Figure 12A and B in the case of high-purity Duran® glass samples with 20 ppm Fe melted under oxidizing (12A) and reducing (12B) conditions (transmission spectra in Figure 8A), and radiated with different sources. Photo-reduction of Fe^{3+} forming (Fe^{3+}) – electron center defects occurs with lowering the induced absorption (increasing transmission) around 220 nm depending on radiation source. Photo-oxidation of Fe^{2+} to $(Fe^{2+})^+$ hole centers increases the induced absorption around 250 nm (decreases transmission), especially by 193-nm laser irradiation. The saturation effect is mainly dependent on the energy density of the radiation source [13, 14]. Radiation defects are also dependent on refining agents, like As_2O_3, Sb_2O_3, or NaCl [20, 21, 27]. Figure 12C shows the formation of $(Cl_2)^-$ defect center at ~330 nm besides Si- and B-related EC and HC centers. Such type of $(Cl_2)^-$ defect center was detected in FP glasses with 10 mol% $SrCl_2$, too [22].

We found that defect generation and healing behavior is of a very complex nature depending on many factors. The brown coloring due to phosphorous-related defects was also detected after X-ray irradiation of a Yb:SiO_2 glass preform doped with P and Al (Figure 13). The preform was prepared by the CVD process (from j-fiber in Jena). A polished cross-section of the preform with a sample thickness of 0.5 mm was exposed to X-ray irradiation.

A common optical plastic is PMMA (polymethyl methacrylate, acrylic, Plexiglas). UV-PMMA has a high UV transmission with a UV edge ~250 nm, a low density, 1.19 g/cm³, refractive index n_D 1.491, and Abbe number 57.4 [1]. However, most plastics degrade when exposed to UV radiation. We studied UV-PMMA samples (thickness 2 mm) under a XeHg lamp ($\lambda > 260$ nm, energy density ~10 times of solar constant) depending on radiation time. We measured the UV-Vis absorption (Figure 14A)

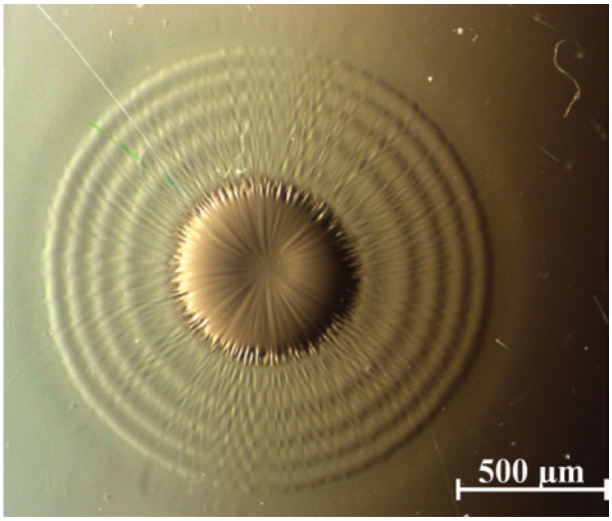

Figure 13: Photograph of a microscopic image of a cross-section of a Yb:SiO_2 glass preform; the core was doped with P and Al, and irradiated with X-ray (thickness of the sample 0.5 mm). The brown coloring of the core is caused by phosphorous-related defects.

and considered the change in sample surface with polarizing microscopy. Already after 15 min, a strong increase in UV absorption was found. Figure 14B shows the kinetics for induced absorption at 300, 350, and 400 nm with measured points and exponential fit (lines). Formation of bubbles and initiation of yellow coloring was observed after 1 h increasing with time of exposure. After 16 h, the surface was destroyed (Figure 14C) by degradation of the organic bonds. Healing was not possible.

6 Summary

The DUV transmission of materials depends on intrinsic electron transitions and extrinsic trace impurities introduced by the raw materials used and the manufacturing process. Fluoride crystals have the highest DUV transmission. Cubic CaF_2 single crystal is the most common optical material for the DUV, especially in optics for

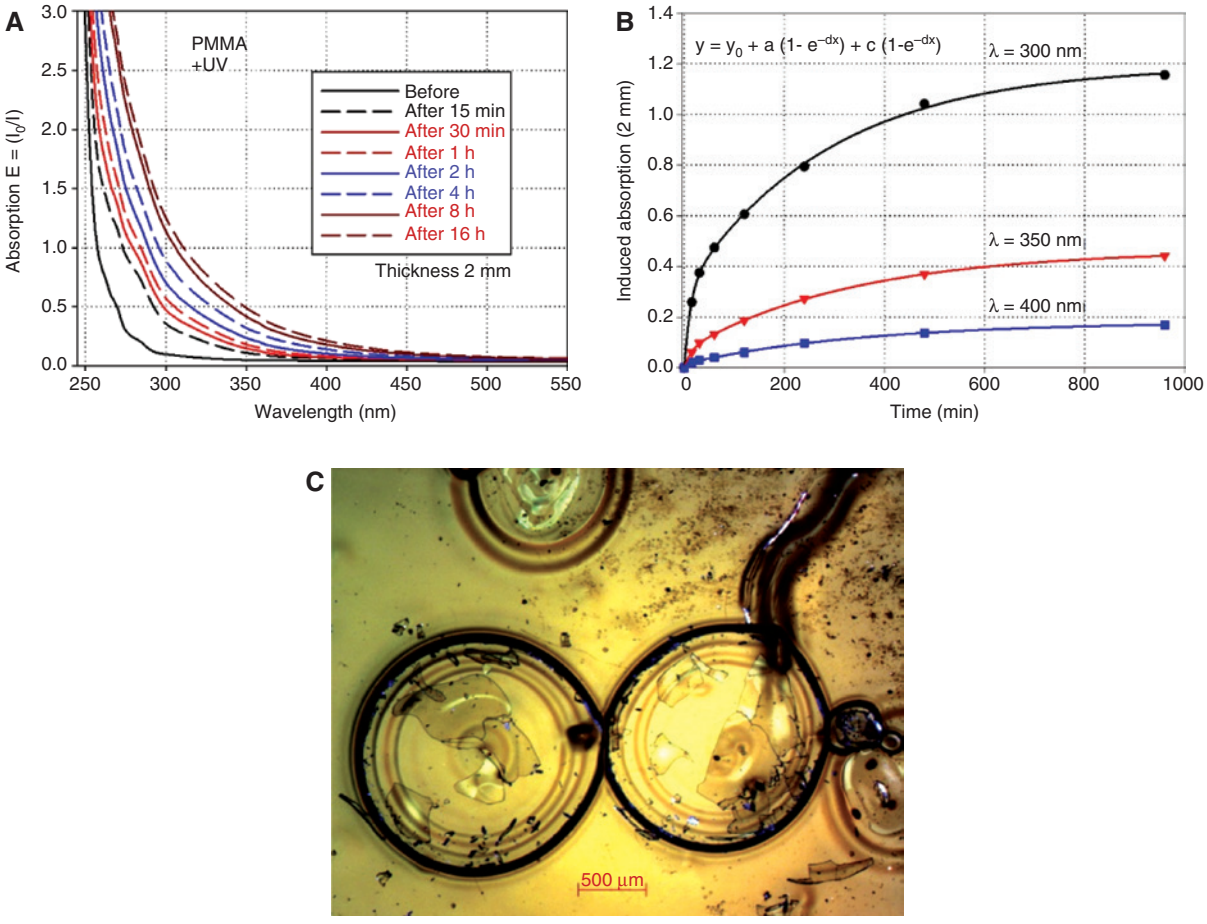

Figure 14: UV PMMA samples exposed to UV light (XeHg lamp with $\lambda > 260$ nm): (A) Induced absorption depending on time. (B) Kinetics of induced absorption at 300, 350, and 400 nm. (C) Photograph image with polarizing microscope after 16 h of exposure shows the total degradation of the sample surface.

microlithography equipment with 193-nm and 248-nm lasers. It is commercially produced in large pieces with extremely high-quality and low radiation damage by UV irradiation. However, crystal growth needs a very long time and all crystals possess typical cleavage behavior, which makes fabricating high-accuracy optical surfaces more difficult. The crystal size of other fluorides, borates, and silicates has been limited until now by the complicated growth process and the lack of useful technologies.

Vitreous silica is an excellent optical material. It is available in large pieces with extremely high purity. The quality is strongly dependent on the raw materials used, natural or synthetic quartzes, or $SiCl_4$ liquid, and the fabricating process. The influence of intrinsic and extrinsic effects on DUV absorption was considered, e.g. of trace impurities, ODC(I), ODC(II), OH, Cl′, F′. The fabrication process for synthetic SiO_2 glass of different types was strongly optimized for various applications. Vitreous silica has many advantages; however, one disadvantage is the high melting temperature and very high viscosity, which limits the homogenization and the distribution of added components.

Special fluoride (FP) and phosphate (P) glasses are attractive candidates for the DUV range, too. The intrinsic UV absorption edges of AlF_3-based glasses are comparable with those of SiO_2. The UV edge of the FP glasses shifted to a longer wavelength with increasing phosphate content. However, the experimental UV transmission of FP glasses is frequently limited by extrinsic absorption due to trace impurities, mainly Fe′, Cu′, Pb^{2+}, and other polyvalent metals with high specific absorption coefficients dependent on the redox state of the ions. The absorption coefficients in the DUV of the lower redox states, Fe^{2+} and Cu^{+}, are more than one order lower than those of the higher redox states, Fe^{3+} and Cu^{2+}. Therefore, the UV transmission can be strongly increased by melting FP and P glasses under reducing conditions, e.g. in carbon crucibles under protective gas.

The optical basicity and optical values were correlated with UV transmission edge (bandgap) and radiation damage. Multicomponent borosilicate glass of Duran® or Pyrex® type have intrinsic transmission, too, due to their special network structure nearly without nonbridging oxygens (NBO). However, the real UV transmission is limited in an analogous way like in multicomponent AlF_3-based FP or phosphate glasses by trace impurities, mainly Fe^{3+}/Fe^{2+}, which are nearly unavoidable in the ppm range by the available raw materials. Photo-ionization processes decrease the UV transmission in several ways much stronger than in high purity silica glasses by the formation of electron center and hole center defects. Most of them could be healed by thermal treatment.

Organic material, UV-PMMA, was destroyed by UV radiation after a short time.

Acknowledgments: The author wishes to thank especially Rotraud Atzrodt for her assistance over a very long time, as well as all her co-workers and students for their support. This work was supported by BMBF grant numbers 03M2713D8, AWO 223895L, DFG EH140, SCHOTT AG, and HERAEUS.

References

[1] M. J. Weber, 'Handbook of Optical Materials', (CRC Press LLC, New York, 2003).
[2] D. Ehrt and W. Seeber, J. Non-Cryst. Solids 129, 19–30 (1991).
[3] P. Shiv Halasyamani and W. Zhang, Inorg. Chem. 56, 12077–12085 (2017).
[4] R. Brückner, 'Silicon Dioxide, Encyclopedia of Appl. Phys. 8', (VCH Publisher Inc., New York, 1997).
[5] D. Ehrt, Proc. SPIE 1761, 213–222 (1992).
[6] D. Ehrt, M. Carl, T. Kittel, M. Müller and W. Seeber, J. Non-Cryst. Solids 177, 405–419 (1994).
[7] D. Ehrt, Phys. Chem. Glasses Eur. J. Glass Sci. Technol. B 56, 217–234 (2015).
[8] D. Ehrt, M. Leister and A. Matthai, Molten Salt Forum 5–6, 547–554 (1998).
[9] H. Ebendorff-Heidepriem and D. Ehrt, Opt. Mater. 15, 7–25 (2000).
[10] D. Ehrt, P. Ebeling and U. Natura, J. Non-Cryst. Solids 263–264, 240–250 (2000).
[11] D. Ehrt, J. Non-Cryst. Solids 196, 304–308 (1996).
[12] D. Ehrt, A. Matthai and M. Leister, Phys. Chem. Glasses 42, 231–239 (2001).
[13] D. Ehrt, P. Ebeling, U. Natura, U. Kolberg, K. Naumann, et al., in 'Proc. Int. Congr. Glass I. Invited Papers', Edinburgh, Scotland, 1–6 July 2001, pp. 84–93.
[14] D. Ehrt, C. R. Chim. 5, 679–692 (2002).
[15] D. Ehrt, J. Non-Cryst. Solids 348, 22–29 (2004).
[16] D. Ehrt and A. Herrmann, Verre 11, 13–18 (2005).
[17] J. A. Duffy and M. D. Ingram, J. Am. Chem. Soc. 93, 6448 (1971); J. Non-Cryst. Solids 21, 373 (1976); in 'Optical Properties of Glass', Ed. By D. R. Uhlmann and N. J. Kreidl (American Ceramic Society, Westerville, OH, 1991) pp. 159–184.
[18] J. A. Duffy, M. D. Ingram and S. Fong, Phys. Chem. Chem. Phys. 2, 1829–1833 (2000).
[19] L. L. Velli, C. P. E. Varsamis, E. I. Kamitsos, D. Möncke and D. Ehrt, Phys. Chem. Glasses Eur. J. Glass Sci. Technol. B 49, 182–187 (2008).
[20] U. Natura and D. Ehrt, Glass Sci. Technol. 72, 295–301 (1999).
[21] U. Natura, D. Ehrt and K. Naumann, Glass Sci. Technol. 74, 23–31 (2001).
[22] P. Ebeling, D. Ehrt and M. Friedrich, Phosphorus Res. Bull. 10, 484–489 (1999).

[23] U. Natura, T. Feurer and D. Ehrt, Nucl. Instrum. Methods Phys. Res. B 166–167, 470–475 (2000).
[24] U. Natura and D. Ehrt, Nucl. Instrum. Methods. Phys. Res. B 174, 143–150 (2001).
[25] U. Natura and D. Ehrt, Nucl. Instrum. Methods Phys. Res. B 174, 151–158 (2001).
[26] D. Ehrt, Glass Technol. 41, 182–185 (2000).
[27] D. Ehrt and P. Ebeling, Glass Technol. 44, 46–49 (2003).
[28] D. Möncke and D. Ehrt, in 'Materials Science Research Horizons', Ed. by H. P. Glick, (Nova Science Publisher, Inc., New York, 2007) pp. 1–56.
[29] D. Möncke, Int. J. Appl. Glass Sci. 6, 1–19 (2015), DOI: 10.1111/ijag.12135.
[30] U. Natura, D. Keutel, M. Letz, L. Parthier and K. Knapp, Proc. SPIE 6520, 652030, 1–4 (2007).
[31] A. Burkert, D. Keutel and U. Natura, Proc. SPIE 6720, 67201K, 1–5 (2007).
[32] U. Natura, S. Rix, M. Letz and L. Parthier, Proc. SPIE 7504, Laser-Induced Damage in Optical Materials: 2009, 75041P (31 December 2009), DOI: 10.1117/12.836409.
[33] H.-D. Witzke, A. Schreiber, U. Klett and B. Uebbing, in 'Proc. XIX Int. Congr. Glass Edinburgh 1–6 July 2001', Phys. Chem. Glasses 43C, 155–158 (2002).
[34] A. Schreiber, B. Kühn, E. Arnold, F.-J. Schilling and H.-D. Witzke, J. Phys. D Appl. Phys. 38, 3242–3250 (2005).
[35] M. Stamminger, Phys. Chem. Glasses Eur. J. Glass Sci. Technol. B 57, 15–20 (2016).
[36] U. Natura, O. Sohr, R. Martin, M. Kahlke and G. Fasold, Proc. SPIE 5273, 155–163 (2003).
[37] U. Natura, O. Sohr, M. Letz, R. Martin, M. Kahlke, et al., Proc. SPIE 5377, 1708–1714 (2004).
[38] U. Natura, R. Martin, G. Goenna, M. Kahlke and G. Fasold, Proc. SPIE 5754, 1312–1319 (2005).
[39] A. Burkert, W. Triebel, U. Natura and R. Martin, Phys. Chem. Glasses Eur. J. Glass Sci. Technol. B 48, 107–112 (2007).
[40] B. Kühn, B. Uebbing, M. Stamminger, I. Radosevic and S. Kaiser, J. Non-Cryst. Solids 130, 23–32 (2003).
[41] D. Möncke and D. Ehrt, Glass Sci. Technol. 75, 163–173 (2002).
[42] D. Möncke and D. Ehrt, Glass Sci. Technol. 75, 243–253 (2002).
[43] D. Möncke, D. Ehrt, H. Eckert and V. Mertens, Glass Technol. 44, 113–116 (2003).
[44] D. Ehrt, in '14th Conf. on Glass & Ceramics', Varna, Bulgaria, 24–28 Sept. 2002, Proc. Vol. 1, pp. 152–157.
[45] T. Kloss, G. Lautenschläger and K. Schneider, Glass Technol. 41, 177–181 (2000).
[46] A. Schütz, D. Ehrt, M. Dubiel, X. C. Yang, B. Mosel, et al., Glass Sci. Technol. 77, 295–305 (2004).
[47] D. Ehrt, Phys. Chem. Glasses Eur. J. Glass Sci. Technol. B 49, 68–72 (2008).
[48] D. Ehrt, IOP Conf. Ser. Mater. Sci. Eng. 21, 012001 (2011).
[49] D. Möncke, G. Tricot, D. Ehrt and E. I. Kamitsos, J. Chem. Tech. Metall. 50, 381–386 (2015).
[50] D. Möncke, G. Tricot, A. Winterstein, D. Ehrt and E. I. Kamitsos, Phys. Chem. Glasses Eur. J. Glass Sci. Technol. B 58, 171–178 (2017).
[51] A. P. Howers, N. M. Vedishcheva, A. Samoson, J. V. Hanna, M. E. Smith, et al., Phys. Chem. Chem. Phys. 3, 11919–11928 (2011).
[52] G. Tricot, Phys. Chem. Chem. Phys. 18, 26764–26770 (2016).
[53] A. Molchanov, U. Hilburger, J. Friedrich, M. Finkbeiner, G. Wehrhan, et al., Cryst. Res. Technol. 37, 77–82 (2002).
[54] L. Skuja, J. Non-Cryst. Solids 239, 16–48 (1998).
[55] M. C. Paul, R. Sen, R. E. Youngman and A. Dhar, J. Non-Cryst. Solids 354, 5408–5420 (2008).
[56] R. E. Youngman and S. Sen, J. Non-Cryst. Solids 337, 182–186 (2004).
[57] A. N. Trukhin, M. F. Kink, Y. A. Maksimov, R. A. Kink, T. A. Ermolenko, et al., J. Non-Cryst. Solids 342, 25–31 (2004).
[58] J. Kirchhof and S. Unger, J. Non-Cryst. Solids 354, 540–545 (2008).
[59] D. Ehrt and R. Keding, Phys. Chem. Glasses Eur. J. Glass Sci. Technol. B 50, 165–171 (2009).
[60] D. Möncke, D. Ehrt and E. I. Kamitsos, Phys. Chem. Glasses Eur. J. Glass Sci. Technol. B 54, 42–51 (2013).
[61] D. Ehrt, H. Reiß and W. Vogel, Silikattechnik 27, 304–309 (1976).
[62] D. Ehrt, H. Reiß and W. Vogel, Silikattechnik 28, 359–364 (1977).
[63] A. Herrmann, S. Fibikar and D. Ehrt, J. Non-Cryst. Solids 355, 2093–2101 (2009).
[64] D. Ehrt, Phys. Chem. Glasses Eur. J. Glass Sci. Technol. B 47, 669–674 (2006).
[65] D. Möncke and D. Ehrt, Opt. Mater. 25, 425–437 (2004).
[66] D. Möncke and D. Ehrt, Phys. Chem. Glasses Eur. J. Glass Sci. Technol. B 48, 317–323 (2007).